Article

Preparation and Optimization of Mesoporous SnO$_2$ Quantum Dot Thin Film Gas Sensors for H$_2$S Detection Using XGBoost Parameter Importance Analysis

Jianqiao Liu [iD], **Yujia Wang, Yue Sun, Kuanguang Zhang, Yang Ding, Ce Fu * and Junsheng Wang**

College of Information Science and Technology, Dalian Maritime University, Dalian 116026, China; jqliu@dlmu.edu.cn (J.L.); wyj118222@163.com (Y.W.); s1120210236@dlmu.edu.cn (Y.S.); zhangkg@dlmu.edu.cn (K.Z.); 2220183190@dlmu.edu.cn (Y.D.); wangjsh@dlmu.edu.cn (J.W.)
* Correspondence: fu_ce@dlmu.edu.cn

Abstract: Tin oxide (SnO$_2$) is a traditional gas-sensitive semiconductor with excellent response to various gases. However, its sensor performances are attenuated by the utility factor during gas diffusion in the sensing body. Therefore, the rational design of microstructure of devices is attractive and necessary because it may provide a sensible and controllable microstructure, which facilitates gas diffusion and inhibits the utility factor. Herein, the mesoporous tin oxide (MPTD) quantum dot thin film for H$_2$S gas sensors is prepared by a facile route, which creates a mesoporous microstructure for thin films by the thermal decomposition of NH$_4$Cl. The pore size of the thin films is controlled to be 19.36–40.13 nm. The mesoporous microstructure exhibits enhanced gas-sensing properties amounting to a 30-fold increase in response and 1/3 reduction in recovery time in H$_2$S detection at room temperature (25 °C), with a limit of detection of 0.4 ppm. To determine the importance of sensor parameters such as pore size, film thickness, and grain size, an eXtreme Gradient Boosting (XGBoost) algorithm model was developed to examine the feature importance of each parameter on the gas-sensing performance of the MPTD sensors. The visual illustration of parameter importance is revealed to facilitate the optimization of technical preparation parameters as well as the rational design of semiconductor gas sensors.

Keywords: mesoporous microstructure; SnO$_2$ quantum dot thin film; NH$_4$Cl; XGBoost algorithm; gas sensor

1. Introduction

Hydrogen sulfide (H$_2$S) is a highly versatile reagent extensively utilized in various fields such as the manufacture of fluorescent powders [1], electroluminescence [2], optical conductors [3], synthesis of organic reducing agents [4], metal refining [5], pesticides, medicine [6], and catalyst regeneration [7]. It is a colorless, highly toxic and acidic gas, with a severe nuisance odor and an olfactory threshold of 0.41 ppb [8]. The exposure to low concentrations of H$_2$S, even at ppb level, can lead to numerous health issues like chronic inflammation of the eyes and respiratory tract, corneal ulceration or punctate keratitis, peripheral neuropathy, central autonomic dysfunction, or damage to peripheral nerves [9]. Additionally, it is flammable and explosive [10] so that the real-time monitoring of H$_2$S is crucial to physical and industrial safety. Therefore, it is necessary to develop gas sensors with excellent sensing performance that are able to detect H$_2$S accurately for safety purposes.

Tin oxide (SnO$_2$) is one of the most popular metal oxide semiconductors for gas sensors [11,12]. Since its first invention in 1962 [13] and first application in gas sensors in 1968 [14], SnO$_2$ has always occupied an important position in the development of gas sensors. The detection of a SnO$_2$ gas sensor relies on the surface chemical reaction between chemisorbed oxygen and the target gas, which causes a change in the electrical resistivity of

semicondutive SnO_2. The response of an n-type SnO_2 gas sensor is usually defined as the ratio of its resistance in air (R_a) to the resistance in a reducing gas (R_g). It is known that the composition, structure, and morphology of a sensing body have great impacts its sensing performance [15,16]. However, the response of traditional SnO_2 gas-sensing materials is usually limited.

The grain-size effect offers significant enhancement in the gas-sensing properties of SnO_2 [17]. Therefore, the nanosized semiconductor provides new prospects for gas sensors. Chen [18] prepared Pd-modified Sb-doped SnO_2 nanomaterials by a simple hydrothermal reaction and reduction method, resulting in a response of 9.7 to 100 ppm hydrogen gas at 320 °C. Mao [19] synthesized heterostructured Nb_2O_5/SnO_2 core–shell nanorods by a facile hydrothermal strategy and atomic layer deposition (ALD), resulting in a response value of 4.0 for 20 ppm H_2S gas at 275 °C.

Quantum dots (QDs) are tiny semiconductor particles that exhibit unique optical and electronic properties due to quantum confinement effects. They are typically nanoscale in size, ranging from 1 to 10 nm [20]. They attract the attention of researchers because of their zero-dimensional properties. SnO_2 QDs exhibit the advantages of strong quantum confinement and stable physical and chemical properties. Furthermore, QDs could provide a large specific surface area with extremely abundant surface dangling bonds, which are highly active and are able to interact with target species during detection [21]. However, ultra-small crystallites also produce difficulties for the nanostructures used for gas detection because there are few pores in the sensing body assembled by QDs. Thus, the diffusion of the target gas is restricted and sensor performance is consequently inhibited.

Porous and hollow micro/nano-materials can promote gas diffusion [22,23], provide higher accessible surface for oxygen [24], and offer more active sites for the adsorption–desorption of gas molecules [25,26], thereby enhancing sensing performance. Briefly, a sensible microstructure may facilitate gas-sensing performance by inhibiting the utility factor of a semiconductor [27,28]. Therefore, the rational design of microstructure devices has attracted widespread attention in recent years.

Templates in various forms are usually used in the preparation of a mesoporous sensing body. For example, Yang [29] used hexagonal mesoporous SBA-15 as the template agent and prepared mesoporous Ag_2O/SnO_2 microspheres gas sensors with a pore size of 3.6 nm by nano-casting. This resulted in a response of 57 to 1 ppm H_2S gas at 100 °C and had a low detection limit (*LoD*) of 300 ppb. In addition, Song [30] used scallion roots as biological templates to prepare mesoporous SnO_2 gas sensors, achieving accurate detection of ppb-level H_2S gas in high humidity (RH = 85%). Sun [31] synthesized platinum nanoparticle (NP)-functionalized flower-like mesoporous SnO_2 gas sensors with a high specific surface area (31.6 $m^2 g^{-1}$) and large pore size (32.5 nm) using dual template technology, resulting in a response of 160 to 5 ppm H_2S gas at room temperature and an *LoD* of 100 ppb. Despite the abovementioned development of mesoporous sensors made, there are still some problems that need to be solved. The fabrication processes with templates were usually complex and required highly hazardous reagents. Thus, it is particularly important to develop a facile method to prepare SnO_2 gas sensors with mesoporous microstructures.

The eXtreme gradient boosting (XGBoost) algorithm [32] can produce visualizations like bar plots or heatmaps that display feature importance scores to aid in the interpretation and understanding of the most influential features. Feature importance analysis using XGBoost is able to identify which features are most relevant for making predictions; focus on key factors; reduce the dimensionality of dataset by removing less important features to improve model efficiency and reduce overfitting; and provide insights into the relationships between features and the target variable [33]. Wan [34] proposed a conversion algorithm based on XGBoost, taking column volume, meteorological factors, and near-surface methane concentration obtained by room temperature gas observation satellites as predictive variables, and analyzed the characteristic factors of four ground monitoring sites of the World Greenhouse Gas Center and the importance of methane concentration prediction. Dong [35] evaluated a numerical weather prediction (NWP) bias-correction

method for the Global Ensemble Forecast System V2 forecast based on an XGBoost model. Thus, XGBoost is a valuable tool for feature selection and model interpretation, making it an essential component of many machine learning workflows. It is known that the gas-sensing performances of SnO_2 thin film gas sensors are affected by the properties of the film, which are determined by various technical process parameters during the preparation of devices. The correlations among gas-sensing properties, film factors, and technical process parameters are complex and implicit. Therefore, the complexity and implicity prevent the comprehensive understanding necessary for the design of a fabrication strategy for gas-sensing materials. Thus, the XGBoost algorithm could be beneficial in providing in-depth analysis of the fundamental parameters of semiconductor gas sensors.

In this paper, the synthesis of a SnO_2 QD solution is completed by using tin chloride ($SnCl_2 \cdot 2H_2O$) and thiourea (CH_4N_2S) as precursors. Ammonium chloride (NH_4Cl) is employed to create a mesoporous microstructure during its thermal decomposition. The gas-sensing performance of the mesoporous microstructure tin dioxide (MPTD) and non-porous thin film are evaluated at room temperature. An eXtreme gradient boosting (XGBoost) algorithm model is developed to discuss the feature importance of each parameter on the gas-sensing performance of MPTD sensors to identify the importance and optimization of sensor preparation parameters.

2. Materials and Methods

The preparation procedure of the MPTD gas sensor is illustrated in Figure 1. At first, 2.257 g of $SnCl_2 \cdot 2H_2O$ and 0.077 g of CH_4N_2S were dissolved in 50 mL of deionized water. The mixture was then stirred at a temperature of 25 °C for 24 h to facilitate the hydrolysis and oxidation process [17,36], after which the SnO_2 QD solution was obtained. Then, various amounts of NH_4Cl were added to the synthesized QD solution to control the pore size of the mesoporous thin film. The NH_4Cl to Sn molar ratio was adjusted to 0.1:1, 0.5:1, 1:1, 1.5:1, 2:1, 2.5:1 and 3:1, respectively. SnO_2 QD solutions with various amounts of NH_4Cl were then spin-coated at a speed of 1000 rpm onto alumina substrates with silver interdigital electrodes. The devices were dried at 130 °C for 10 min and the deposition was repeated 2–5 times for film thickness control. Afterwards, the thin film devices were sintered in a muffle furnace at temperatures of 330–370 °C. Among the samples, MPTD-NA1.5 denoted the MPTD thin film gas sensor that was prepared using the following parameters: NH_4Cl addition of 1.5, decomposition at 320 °C for 20 min, and sintering at 330 °C.
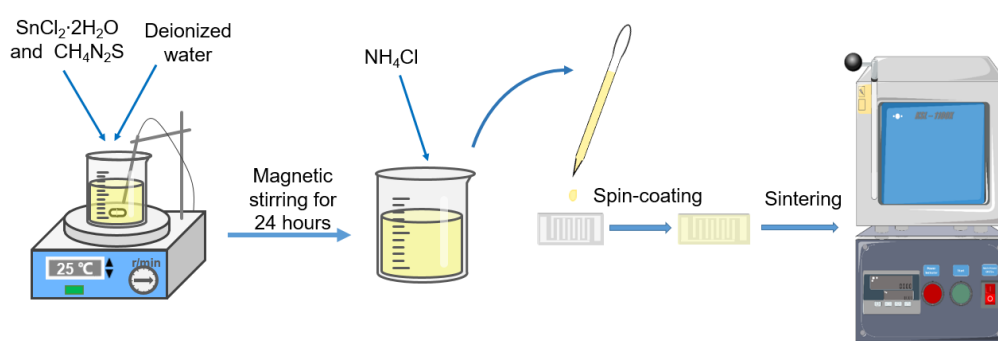
Figure 1. The preparation process of MPTD gas sensors.

The crystal structures of MPTD thin films were characterized by X-ray diffraction (XRD, D/Max-2550, Rigaku, Tokyo, Japan). The thermogravimetric-differential thermal analysis (TG-DTA) was carried out by a simultaneous thermal analyzer (SDT-650, TA Instruments, Dallas, TX, USA). The morphology of the SnO_2 QDs was observed by high-resolution transmission electron microscopy (HRTEM, JEM-3200FS, JEOL, Tokyo, Japan). The surface and profile morphology of the MPTD thin films were carried out using a scanning electron microscope (SEM, SIGMA-500, Carl Zeiss AG, Oberkochen, Germany). The pores of the MPTD films were characterized by a Brunauer–Emmett–Teller (BET, ASAP-

2460, Micromeritics, Atlanta, GA, USA) analyzer using adsorption–desorption isotherms of nitrogen (N_2). The weighted average size of pores was calculated by evaluated pore volume using Barret–Joyner–Halenda (BJH) desorption dV/dlog (D). The electrical resistance of the thin film gas sensor was measured by a WS-30B gas sensor characterization system (Winson, Zhengzhou, China). The characterization was performed by using H_2S as the target gas at room temperature (25 °C) with relative humidity of 40%. The sensor response (*S*) was defined as the ratio of R_a to R_g, as shown in Equation (1).

$$S = R_a / R_g \tag{1}$$

3. Results

3.1. Microstructural, Morphological and Compositional Properties

The XRD pattern of the SnO_2 thin film of the MPTD-NA1.5 gas sensor is exhibited in Figure 2a. The distinct diffraction peaks at 2θ = 26.27°, 33.52°, and 51.78° were observed, corresponding to the (110), (101), and (211) facets of rutile SnO_2, respectively, in good agreement with the standard pattern of rutile SnO_2 (JCPDS Card No. 41-1445) [37]. The lattice parameters of SnO_2 QDs are a = b = 0.4738 nm, c = 0.3187 nm. The average crystallite size is calculated to be 3.08 nm according to the Scherrer's formula [38] based on these main diffraction peaks. The TG-DTA of MPTD thin films is shown in Figure 2b. A significant endothermic peak with shape decrease in weight was observed at 300 °C, demonstrating that the NH_4Cl addition was decomposed into gaseous NH_3 and HCl at this temperature.
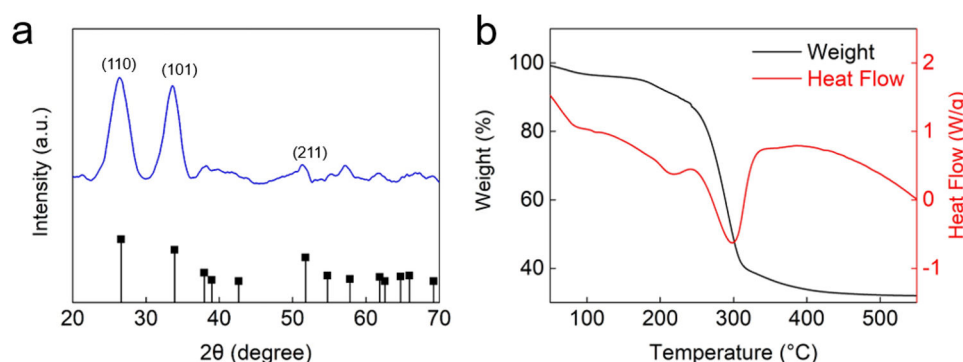
Figure 2. (**a**) XRD pattern and (**b**) TG-DTA of MPTDs thin films.

Figure 3a exhibits SEM surface and profile of the MPTD-NA1.5 thin film. The obvious porous structures with an average pore diameter of 52.16 nm was observed. Figure 3b shows the profiles of the films and their thicknesses were measured to be 290 nm, 331 nm, 542 nm, and 1210 nm. The mesoporous thin films were composed of SnO_2 QDs and their HRTEM morphologies sintered at various temperatures were demonstrated in Figure 4. The grain size of QDs increases with sintering temperature as expected [17]. Specifically, at sintering temperatures of 330 °C, 340 °C, 350 °C, 360 °C, and 370 °C, the corresponding grain sizes were measured to be 2.98 nm, 3.37 nm, 3.57 nm, 3.61 nm, and 3.91 nm, respectively. As shown in Figure 4, the grain size was found to be of positive dependence on sintering temperature, with linear slope of 0.02 nm/°C. The result of MPTD-NA1.5 thin film sintered at 330 °C is very close to the average crystallite size evaluated from the XRD pattern. Thus, the individual grains are probable to be crystallites, which are compose of the SnO_2 QD assembly of thin films. The clear lattice fringes with respective spacings of 0.27 nm and 0.33 nm were observed, corresponding to the (101) and (110) crystal facets of the rutile SnO_2 matrix.

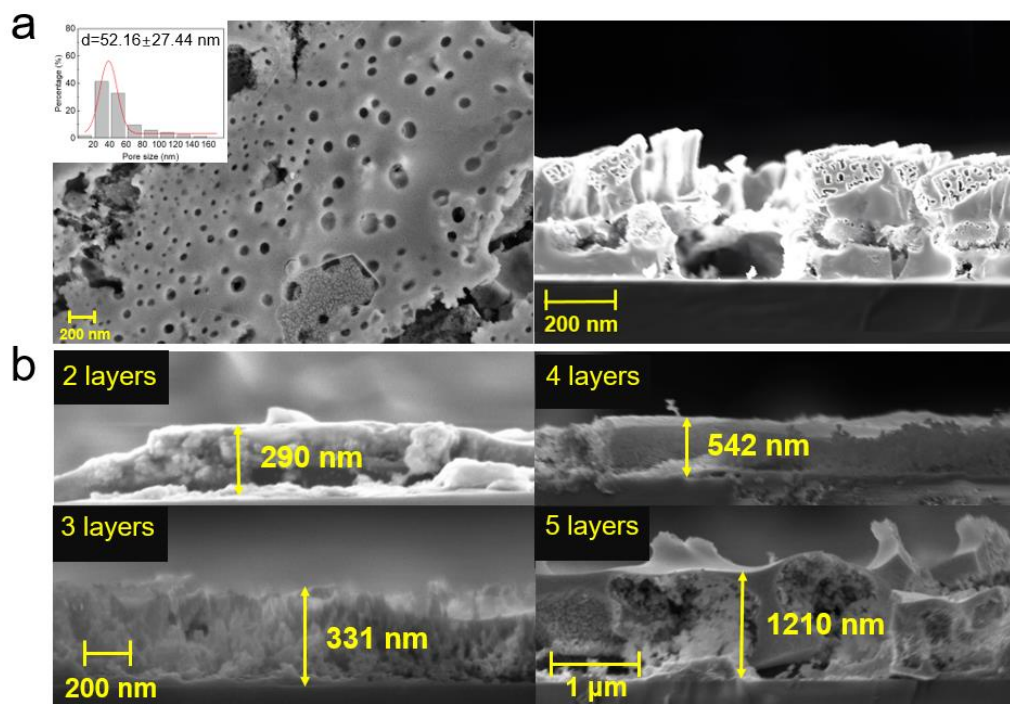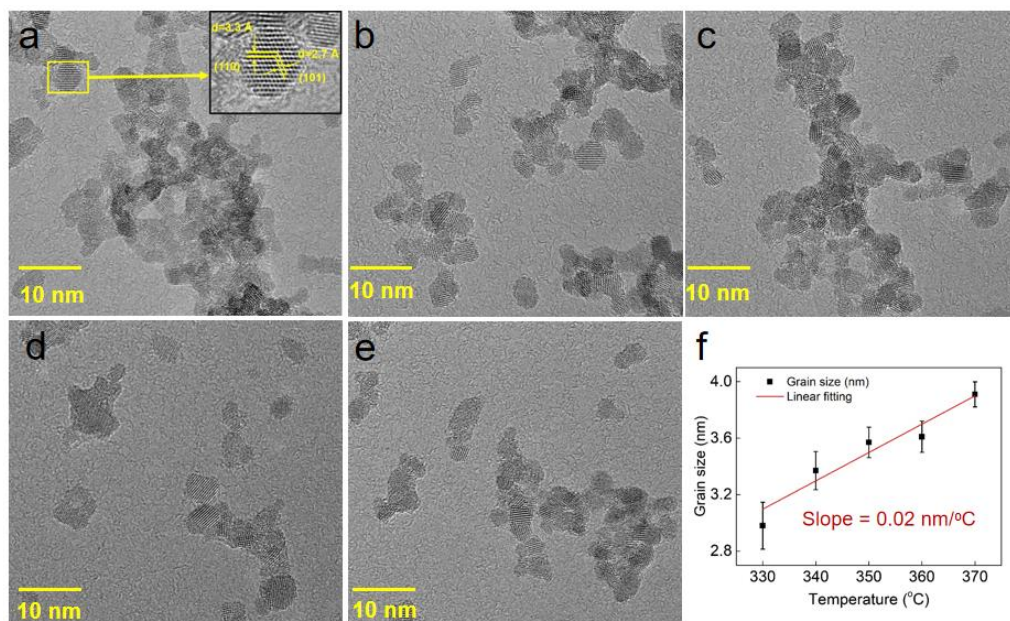**Figure 3.** The SEM images of MPTD: (**a**) surface and profile and (**b**) with various thicknesses.

Figure 4. The HRTEM images of SnO$_2$ QDs with various sintering temperatures: (**a**) 330 °C, (**b**) 340 °C, (**c**) 350 °C, (**d**) 360 °C, and (**e**) 370 °C, (**f**) the dependence of grain size of SnO$_2$ QDs on sintering temperature.

Figure 5 demonstrates the BET adsorption–desorption isotherms of nitrogen as well as the average pore size of the MPTD thin films. The adsorption–desorption isotherms confirm the mesoporous microstructures of thin films. The pore size shows different dependencies on the preparation parameters of the NH$_4$Cl addition, decomposition temperature, and decomposition time. The pore size increases with the NH$_4$Cl addition and reaches a peak when the addition is 1.5 while it begins to decrease when further NH$_4$Cl is incorporated. However, it was observed that the reversal correlations of pore size against the temperature and time of NH$_4$Cl decomposition. The complex dependences of pore size and technical

preparation parameters infer that the mesoporous microstructure of SnO_2 thin films is determined by the decomposition kinetics of NH_4Cl, which is decomposed into gaseous HCl and NH_3 at the temperature above 300 °C. The gaseous resultants create pores in SnO_2 thin films before their escape and leave the mesoporous microstructure of thin films. The mesoporous characteristics are determined by the kinetics of the formation and migration of the gaseous resultants during NH_4Cl decomposition. It is noted that the average pore size of samples observed from the SEM in Figure 3a is different from the one evaluated from BET characterization due to the uneven spatial and dimensional distribution of the pores in the thin films. The results of BET calculations are considered valid and used in further discussions as the BET characterizations reveal the microstructures both on the surface and in the bulk.
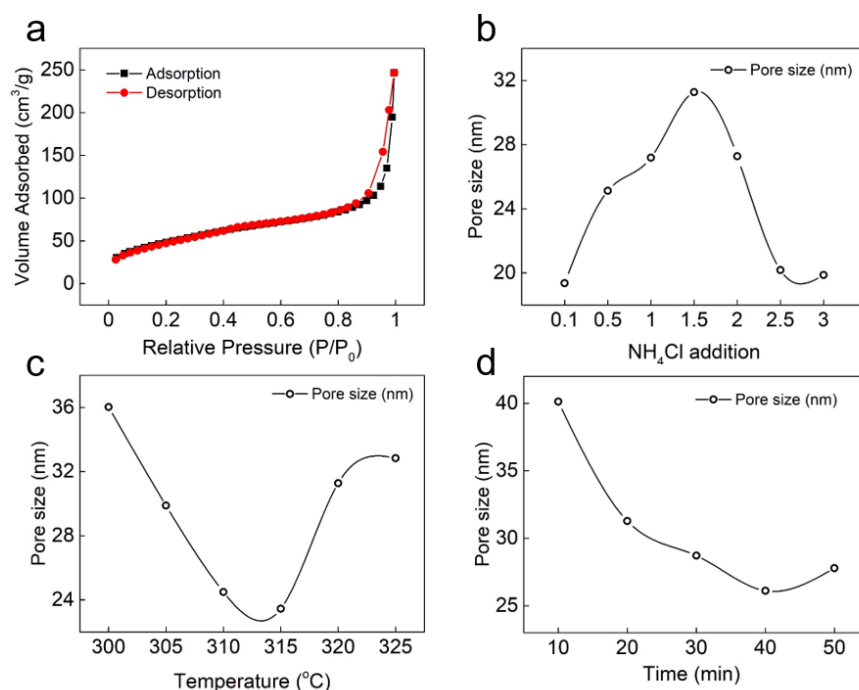

Figure 5. (**a**) Adsorption–desorption isotherms of nitrogen on the MPTDs, the pore sizes of MPTDs under different processes: (**b**) the NH_4Cl addition, (**c**) decomposition temperature, and (**d**) decomposition time.

The chemical and elemental compositions of MPTD thin films were analyzed using XPS spectra, which were calibrated using the C 1s peak at a binding energy of 284.8 eV [39]. The survey spectrum is shown in Figure 6a, which confirms the presence of Sn, O, and C elements. Figure 6b shows the Sn 3d spectra of MPTD thin films with NH_4Cl additions of 0.5, 1.5, and 2, decomposed at 320 °C for 20 min. Two sub-peaks at binding energies of 495.52 eV and 487.21 eV were observed, corresponding to the Sn $3d_{3/2}$ and Sn $3d_{5/2}$ orbitals of Sn elements [40], respectively. As shown in Figure 6c,d, the duration and temperature of NH_4Cl decomposition exhibit minor impacts on the Sn 3d spectra.

The O 1s spectra of MPTD samples are demonstrated in Figures 7 and 8 along with their deconvoluted sub-peaks within the ranges of 530.1–530.8 eV and 531.1–531.9 eV, respectively. The former indicates the lattice oxygen [41] with full coordination with Sn atoms while the latter denotes the chemisorbed oxygen on the surface of SnO_2 QDs [42]. The percentages of chemisorbed oxygen are calculated based on the proportion of sub-peak areas, as shown in Figure 7f. It was found that the incremental decomposition time enhances the chemisorption of oxygen.
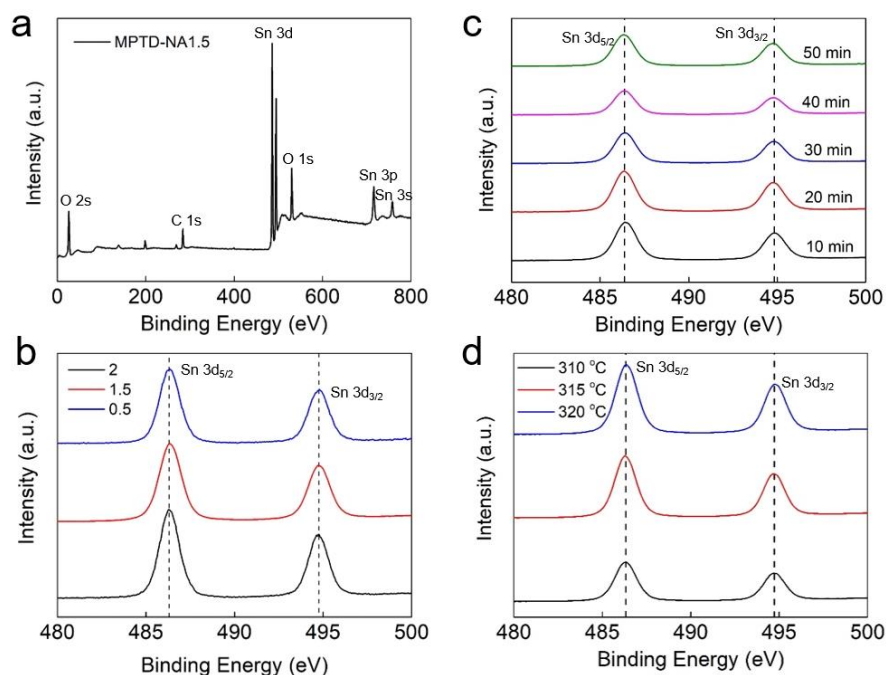
Figure 6. (**a**) The XPS survey spectrum as well as Sn 3d spectra of MPTDs thin films under various technical preparation parameters: (**b**) NH$_4$Cl addition, (**c**) decomposition time, and (**d**) decomposition temperature.
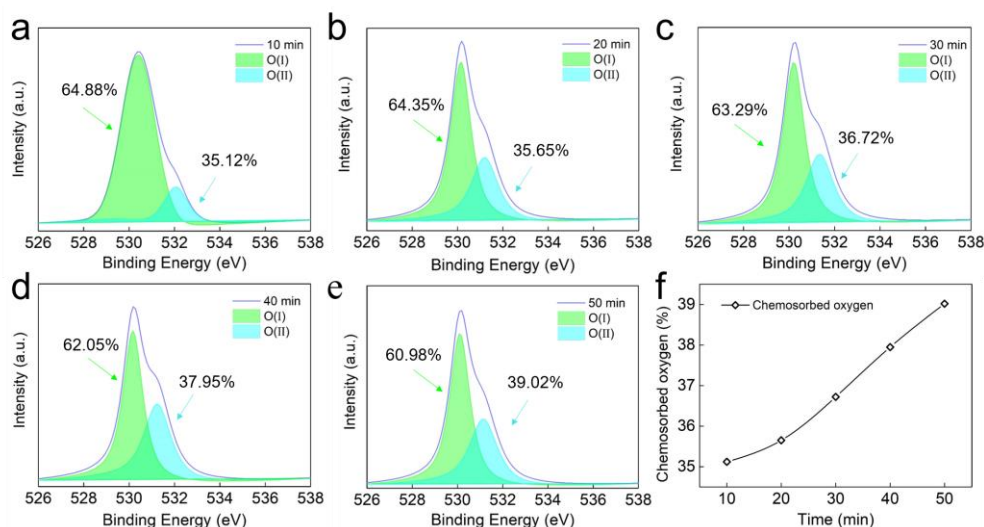
Figure 7. The XPS spectra of O 1s for MPTD thin films with various NH$_4$Cl decomposition times: (**a**) 10 min, (**b**) 20 min, (**c**) 30 min, (**d**) 40 min, and (**e**) 50 min, (**f**) the relationship between the percentage of chemisorbed oxygen and decomposition time.

Meanwhile, the decomposition temperature has the same impact on chemisorbed oxygen. Nevertheless, the NH$_4$Cl addition inhibits the chemisorption of oxygen on the surface. It is noted that the chemisorbed oxygen plays a critical role in the gas-sensing properties of semiconductor sensors [43]. Thus, the technical preparation parameters could determine the performances of gas sensors by imposing complex impacts on the microstructural, morphological, and compositional properties of MPTD thin films.
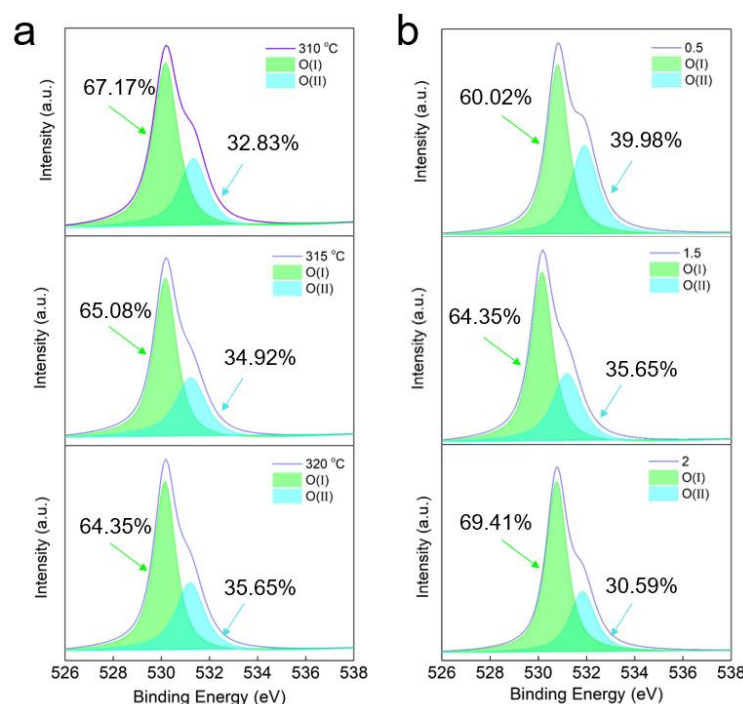
Figure 8. The XPS spectra of O 1s for MPTD thin films with various preparation parameters: (**a**) NH$_4$Cl decomposition temperature and (**b**) NH$_4$Cl addition.

3.2. Gas-Sensing Properties

Figure 9 illustrates the transient responses of the non-porous SnO$_2$ QD thin film gas sensor and the MPTD-NA1.5 gas sensor to 2 ppm H$_2$S at room temperature. The non-porous SnO$_2$ QD film gas sensor demonstrates a response of 4.85, with a response and recovery time of 224/408 s, respectively. In comparison, the MPTD-NA1.5 gas sensor shows a significant enhancement in response, this being 152.9 with a response/recovery time of 225/275 s. It can be concluded that the MPTD gas sensor demonstrates impressive higher response and faster recovery compared to the traditional non-porous SnO$_2$ QD film gas sensor. The 30-fold increase in response and 1/3 reduction in recovery time are ascribed to the mesoporous microstructure of thin films, which facilitate the diffusion of the target gas and therefore its interaction with semiconductor grains. The relationships between pore size of thin films and their gas-sensing properties are exhibited in Figure 10, where the MPTD-NA1.5 thin films with various pore sizes are summarized. The pore size is controlled by NH$_4$Cl additions, decomposition temperatures, and times and the values are extracted from the dependences shown in Figure 5. It is observed that both the electrical resistance and response to 2 ppm H$_2$S of thin film sensors increase with pore size. The present devices derived from MPTD exhibit high resistance at 10^2 MOhm level. It is noted that the thin films are an assembly of SnO$_2$ QDs with crystallite size of 2.98–3.91 nm. However, the width of the depletion layer of the SnO$_2$ semiconductor is considered to be 3–4.2 nm [44,45]. Consequently, all of the QDs composing MPTD thin films are of volume depletion, where free electrons in n-type SnO$_2$ crystallites are seized by aerial oxygen that have a chemical linkage on the semiconductor surface. Despite the high resistance of the present MPTD sensors compared to traditional SnO$_2$ devices, the volume depletion may beneficial to the sensitivity of semiconductor as the depletion layer makes up the dominant part of the sensing body [46,47]. Furthermore, the enhancement in sensor performances could be ascribed to the formation of a mesoporous microstructure, which expands the specific surface area and provides abundant active sites for gas adsorption and desorption [48]. Specifically, the mesoporous microstructure inhibits the utility factor of a semiconductor [27], which describes the gas diffusion in thin films. The pores created by NH$_4$Cl decomposition facilitate the diffusion of the target gas during the adsorption and

desorption processes. Therefore, it is possible to enhance the gas-sensing properties of the thin film by the rational design of the mesoporous microstructure, which inhibits the utility factor of semiconductors.
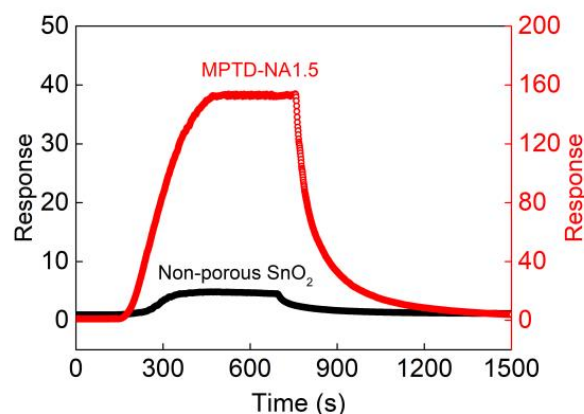

Figure 9. The dynamic responses of nonporous SnO_2 quantum dot thin film gas sensor and MPTD-NA1.5 thin film gas sensor.
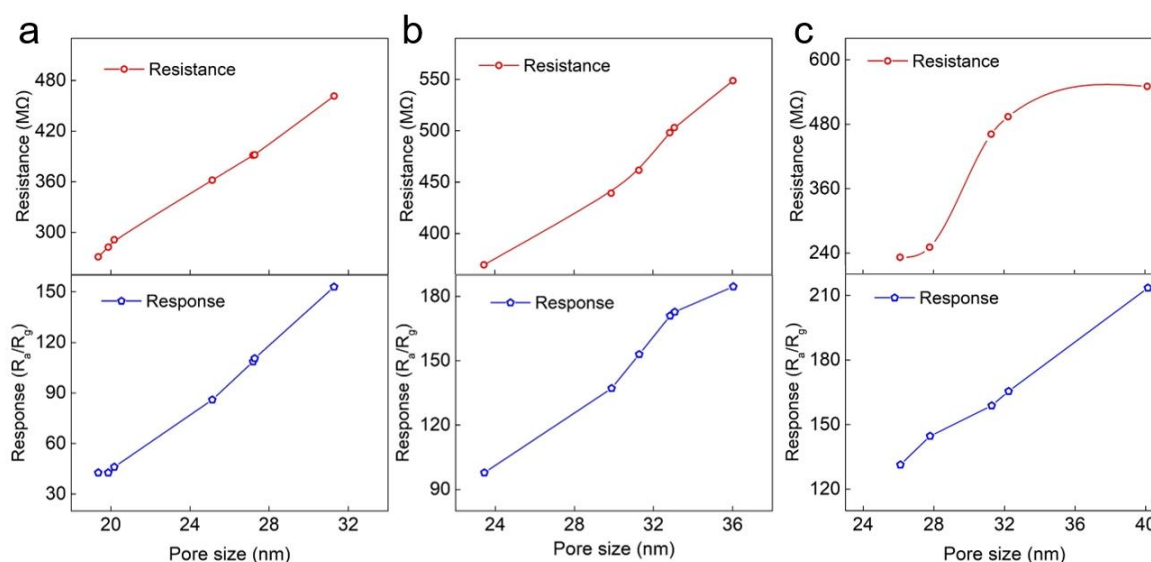
Figure 10. The relationship between pore size and response of MPTD thin film sensors prepared by various technical parameters: (**a**) NH_4Cl addition, (**b**) decomposition temperature, and (**c**) decomposition time.

Figure 11 shows the transient response of the MPTD-NA1.5 thin film gas sensor exposed to 0.4 ppm, 0.8 ppm, 1.2 ppm, 1.6 ppm, and 2 ppm of H_2S gas. The corresponding responses were measured as 26.0, 49.6, 100.1, 136.1, and 152.9, respectively. The response increases with H_2S concentration and it follows a linear relationship in logarithmic coordinates, as shown in Figure 11b. The linearity coefficient indicates a high sensitivity of 1.185 for the thin film sensor. Furthermore, the MPTD thin film exhibits good recovery and repeatability in continuous testing cycle. The response–concentration relationship of the MPTD-NA1.5 thin film gas sensors was investigated to trace H_2S concentration followed by Equation (2):

$$\ln(S) = 1.185 \times \ln(C) + 4.302 \tag{2}$$
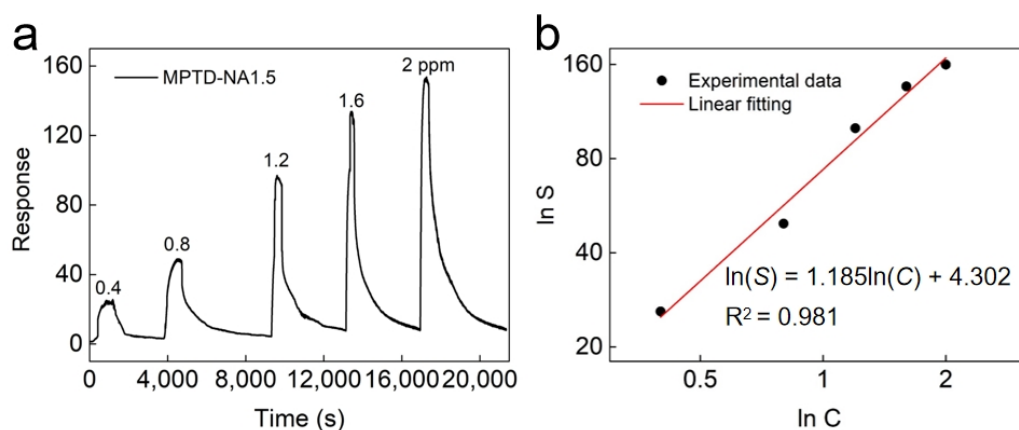
Figure 11. The dynamic response and repeatability of the MPTD-NA1.5 gas sensor: (**a**) dynamic response in 5 repeated test; (**b**) linear fitting of ln*S* against ln*C*.

As shown in Figure 11, the square of the linear correlation coefficient (R^2) was close to 1, showing that the relationship between the response of the MPTD-NA1.5 and the gas concentration varying from 0.4 ppm to 2 ppm is highly linear. The linear correlation allows the evaluation of *LoD* according to Equation (3), where σ represents slope and *SD* represents standard deviation. The theoretical *LoD* of the MPTD-NA1.5 thin film gas sensor is 63 ppb, which has the potential to meet the requirements of ppb-level detection of H_2S. However, it is noted that this *LoD* result has not been not verified because the gas sensor characterization system is not convinced at low concentrations of target gas.

$$LoD = 3\sigma/SD \tag{3}$$

3.3. Feature Importance Analysis of Technical Preparation Parameters

The results discussed above demonstrate that the technical preparation parameters influence the gas-sensing properties of semiconductors by controlling the microstructural, morphological and compositional characteristics of thin films. The correlations are complex among technical preparation parameters, thin film characteristics, and sensor performances because one variable could correlate to another in an explicit or implicit way. However, it is necessary to discover the enhancing mechanism of mesoporous microstructure to gas-sensing properties of thin films. As a versatile and intelligent tool, machine learning can effectively analyze the impacts of various parameters on gas-sensing performance and reveal relationships between the preparation parameters [49]. To identify the feature importance of parameters in the sensor preparation process, the eXtreme gradient boosting (XGBoost) model was used based on the experimental dataset of gas-sensing properties. Thus, it was possible to identify the preparation parameter that had the greatest impact on gas sensitivity for the rational design of microstructure of thin films. During the preparation process of a gas sensor, there are five critical parameters that make significant impacts on the electrical resistance (R_a) of the thin film, such as the NH_4Cl addition (Addition), NH_4Cl decomposition temperature (Tem1), NH_4Cl decomposition time (Time), sintering temperature (Tem2), and coating layers (Layer). To determine the feature importance scores of these parameters on R_a, the XGBoost algorithm was used for visual illustrations, as shown in Figure 12a. It indicated that sintering temperature has the greatest impact on R_a, with a feature importance score of 0.46, while the NH_4Cl addition has the least impact, with a feature importance score of 0.002. Figure 12b shows the correlation heatmap of the five parameters, indicating their independent influences on the sensor properties. Similarly, the dependences of five preparation parameters above on the sensor response (S) were analyzed by the XGBoost algorithm. Figure 12c reveals that sintering temperature has the most substantial impact on S, with a feature importance score of 0.71, whereas the NH_4Cl addition and coating layers have minor impacts, with feature importance scores of 0.002 and 0.004, respectively. The correlation heatmap of five parameters is shown in

Figure 12d, indicating their relative independence during sensor preparation. Therefore, it was found that the sintering temperature, decomposition time, and temperature are the top three parameters that are crucial to the gas-sensing properties of MPTD gas sensors. These parameters are the key factors in the rational design of mesoporous thin films. Furthermore, the XGBoost model was able to provide the optimization of technical preparation parameters, which are NH_4Cl addition of 1.5, NH_4Cl decomposition temperature of 300 °C, NH_4Cl decomposition time of 10 min, sintering temperature of 370 °C as well as film layers of 2, for the optimal gas-sensing performances of MPTD sensors.
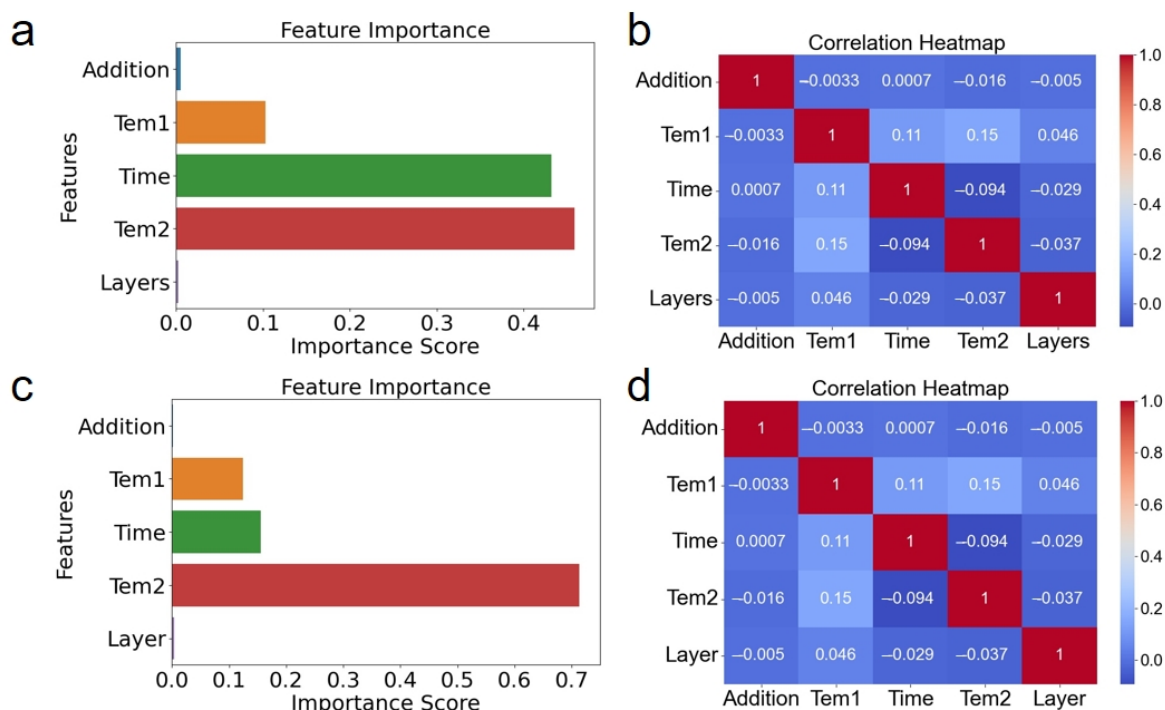
Figure 12. The preparation parameters influcing the electrical resistance of MPTD gas sensors: (**a**) feature importance graph and (**b**) correlation heatmap. The preparation parameters influcing the response of MPTD gas sensors: (**c**) feature importance graph and (**d**) correlation heatmap.

The optimized technical preparation parameters would allow rational design of microstructure of SnO_2 gas sensors. However, the universal deficiencies of semiconductor devices are still an area of concern, such as humidity dependence and baseline drift in practical applications. The present MPTD thin films comprised tiny QDs, which are volume-depleted. The volume depletion would be beneficial to address the problems as it restricts the quantity of adsorbed oxygen on surface of crystallites. Nevertheless, further investigations are expected to provide in-depth understanding on these matters.

4. Conclusions

The MPTD thin film gas sensors are designed and prepared by using various technical preparation parameters such as the NH_4Cl addition, NH_4Cl decomposition temperature and time, sintering temperature, and spin-coating layers. The fabricated MPTD gas sensors have pore size of 19.36–40.13 nm, grain size of 2.98–3.91 nm and film thickness of 290–1210 nm. Compared to non-porous SnO_2 QD thin films, the MPTD sensors own a larger specific surface area, which contributes to their superior gas sensing performances by inhibiting the utility factor of semiconductors. The mesoporous microstructure of the sensors provides a 30-fold increase in response and 1/3 reduction in recovery time as well as lower detection limit of 0.4 ppm for H_2S detection, demonstrating their strong potential for use in gas sensing applications. Additionally, the XGBoost model is employed to analyze the feature importance of the technical preparation parameters. The parameters

that have the greatest impact on the gas-sensing properties were identified. Therefore, the results contribute to the optimization of technical preparation parameters as well as the rational design of semiconductor gas sensors.

References

1. Chen, S.; Zhang, Y.; Wu, M.; Fang, W.; Yang, Y. Study on methanethiol synthesis from H2S and dimethyl sulfide over Al2O3 catalysts promoted with phosphorus. *Appl. Catal. A Gen.* **2012**, *431*, 151–156. [CrossRef]
2. Morishita, T.; Matsuyama, H.; Matsui, M.; Tonomura, S.; Wakihara, M. Distribution of luminescent centers in electroluminescent SrS: Ce films prepared by post-annealing in H2S. *Appl. Surf. Sci.* **2000**, *157*, 61–66. [CrossRef]
3. Cheroff, G.; Keller, S.P. Optical transmission and photoconductive and photovoltaic effects in activated and unactivated single crystals of ZnS. *Phys. Rev.* **1958**, *111*, 98. [CrossRef]
4. Keefe, A.D.; Miller, S.L.; Mcdonald, G.; Bada, J. Investigation of the prebiotic synthesis of amino acids and RNA bases from CO2 using FeS/H2S as a reducing agent. *Proc. Natl. Acad. Sci. USA* **1995**, *92*, 11904–11906. [CrossRef]
5. Dernehl, C.U.; Stead, F.M.; Nau, C.A. Arsine, Stibine, and Hydrogen Sulfide: Accidental Generation in a Metal Refinery. *Am. Ind. Hyg. Assoc. Q.* **1944**, *5*, 361–362.
6. Jacob, C.; Anwar, A.; Burkholz, T. Perspective on recent developments on sulfur-containing agents and hydrogen sulfide signaling. *Planta Medica* **2008**, *74*, 1580–1592. [CrossRef]
7. Wachter, P.; Gaber, C.; Raic, J.; Demuth, M.; Hochenauer, C. Experimental investigation on H2S and SO2 sulphur poisoning and regeneration of a commercially available Ni-catalyst during methane tri-reforming. *Int. J. Hydrog. Energy* **2021**, *46*, 3437–3452. [CrossRef]
8. Sarfraz, J.; Rosqvist, E.; Ihalainen, P.; Peltonen, J. Electro-Optical Gas Sensor Consisting of Nanostructured Paper Coating and an Ultrathin Sensing Element. *Chemosensors* **2019**, *7*, 23. [CrossRef]
9. Jensen, A.R.; Drucker, N.A.; Khaneki, S.; Ferkowicz, M.J.; Yoder, M.C.; Deleon, E.R.; Olson, K.R.; Markel, T.A. Hydrogen sulfide: A potential novel therapy for the treatment of ischemia. *Shock Inj. Inflamm. Sepsis Lab. Clin. Approaches* **2017**, *48*, 511–524. [CrossRef]
10. Motaung, D.E.; Mhlongo, G.H.; Bolokang, A.S.; Dhonge, B.P.; Swart, H.C.; Ray, S.S. Improved sensitivity and selectivity of pristine zinc oxide nanostructures to H2S gas: Detailed study on the synthesis reaction time. *Appl. Surf. Sci.* **2016**, *386*, 210–223. [CrossRef]
11. Liu, J.; Zhang, C.; Wang, Y.; Chen, X.; Jing, R.; Song, T.; Zhang, Z.; Wang, H.; Fu, C.; Wang, J.; et al. Black phosphorus nanodot incorporated tin oxide hollow-spherical heterojunction for enhanced properties of room-temperature gas sensors. *Ceram. Int.* **2023**, *49*, 8248–8258. [CrossRef]
12. Liu, J.; Zhang, Q.; Tian, X.; Hong, Y.; Nie, Y.; Su, N.; Jin, G.; Zhai, Z.; Fu, C. Highly efficient photocatalytic degradation of oil pollutants by oxygen deficient SnO2 quantum dots for water remediation. *Chem. Eng. J.* **2021**, *404*, 127146. [CrossRef]
13. Seiyama, T.; Kato, A.; Fujiishi, K.; Nagatani, M. A new detector for gaseous components using semiconductive thin films. *Anal. Chem.* **1962**, *34*, 1502–1503. [CrossRef]
14. Matsuura, Y.; Takahata, K.; Ihokura, K. Mechanism of gas sensitivity change with time of SnO2 gas sensors. *Sens. Actuators* **1988**, *14*, 223–232. [CrossRef]
15. Wang, X.; Fan, H.; Ren, P. Self-assemble flower-like SnO2/Ag heterostructures: Correlation among composition, structure and photocatalytic activity. *Colloids Surf. A Physicochem. Eng. Asp.* **2013**, *419*, 140–146. [CrossRef]
16. Chen, J.S.; Lou, X.W. SnO2-based nanomaterials: Synthesis and application in lithium-ion batteries. *Small* **2013**, *9*, 1877–1893. [CrossRef]
17. Liu, J.; Lv, J.; Shi, J.; Wu, L.; Su, N.; Fu, C.; Zhang, Q. Size effects of tin oxide quantum dot gas sensors: From partial depletion to volume depletion. *J. Mater. Res. Technol.* **2020**, *9*, 16399–16409. [CrossRef]
18. Chen, X.; Liu, T.; Wu, R.; Yu, J.; Yin, X. Gas sensors based on Pd-decorated and Sb-doped SnO2 for hydrogen detection. *J. Ind. Eng. Chem.* **2022**, *115*, 491–499. [CrossRef]

19. Mao, L.-W.; Zhu, L.-Y.; Tao Wu, T.; Xu, L.; Jin, X.-H.; Lu, H.-L. Excellent long-term stable H2S gas sensor based on Nb2O5/SnO2 core-shell heterostructure nanorods. *Appl. Surf. Sci.* **2022**, *602*, 154339. [CrossRef]

20. Keshtkar, S.; Rashidi, A.; Kooti, M.; Askarieh, M.; Pourhashem, S.; Ghasemy, E.; Izadi, N. A novel highly sensitive and selective H$_2$S gas sensor at low temperatures based on SnO$_2$ quantum dots-C(60) nanohybrid: Experimental and theory study. *Talanta Int. J. Pure Appl. Anal. Chem.* **2018**, *188*, 531–539.

21. Xia, Z.; Zheng, C.; Hu, J.; Yuan, Q.; Zhang, C.; Zhang, J.; He, L.; Gao, H.; Jin, L.; Chu, X.; et al. Synthesis of SnO$_2$ quantum dot sensitized LaFeO$_3$ for conductometric formic acid gas sensors. *Sens. Actuators B Chem.* **2023**, *379*, 133198. [CrossRef]

22. Wang, L.; Fei, T.; Deng, J.; Lou, Z.; Wang, R.; Zhang, T. Synthesis of rattle-type SnO2 structures with porous shells. *J. Mater. Chem.* **2012**, *22*, 18111–18114. [CrossRef]

23. Zhao, Y.; Jiang, L. Hollow micro/nanomaterials with multilevel interior structures. *Adv. Mater.* **2009**, *21*, 3621–3638. [CrossRef]

24. Liu, J.; Lu, Y.; Cui, X.; Geng, Y.; Jin, G.; Zhai, Z. Gas-sensing properties and sensitivity promoting mechanism of Cu-added SnO2 thin films deposited by ultrasonic spray pyrolysis. *Sens. Actuators B Chem.* **2017**, *248*, 862–867. [CrossRef]

25. Zhang, J.; Jia, X.; Lian, D.; Yang, J.; Wang, S.; Li, Y.; Song, H. Enhanced selective acetone gas sensing performance by fabricating ZnSnO3/SnO2 concave microcube. *Appl. Surf. Sci.* **2021**, *542*, 148555. [CrossRef]

26. Lian, X.X.; Li, Y.; Zhu, J.; Zou, Y.; Liu, X.; An, D.; Wang, Q. Synthesis of coryphantha elephantidens-like SnO2 nanospheres and their gas sensing properties. *Curr. Appl. Phys.* **2019**, *19*, 849–855. [CrossRef]

27. Sakai, G.; Matsunaga, N.; Shimanoe, K.; Yamazoe, N. Theory of gas-diffusion controlled sensitivity for thin film semiconductor gas sensor. *Sens. Actuators B Chem.* **2001**, *80*, 125–131. [CrossRef]

28. Liu, J.; Gong, S.; Xia, J.; Quan, L.; Liu, H.; Zhou, D. The sensor response of tin oxide thin films to different gas concentration and the modification of the gas diffusion theory. *Sens. Actuators B Chem.* **2009**, *138*, 289–295. [CrossRef]

29. Yang, T.; Yang, Q.; Xiao, Y.; Sun, P.; Wang, Z.; Gao, Y.; Ma, J.; Sun, Y.; Lu, G. A pulse-driven sensor based on ordered mesoporous Ag2O/SnO2 with improved H2S-sensing performance. *Sens. Actuators B Chem.* **2016**, *228*, 529–538. [CrossRef]

30. Song, B.; Zhang, M.; Teng, Y.; Zhang, X.; Deng, Z.; Huo, L.; Gao, S. Highly selective ppb-level H2S sensor for spendable detection of exhaled biomarker and pork freshness at low temperature: Mesoporous SnO2 hierarchical architectures derived from waste scallion root. *Sens. Actuators B Chem.* **2020**, *307*, 127662. [CrossRef]

31. Sun, Y.; Zhao, Y.; Sun, H.; Jia, F.; Kumar, P.; Liu, B. Synthesis and room-temperature H2S sensing of Pt nanoparticle-functionalized SnO2 mesoporous nanoflowers. *J. Alloys Compd.* **2020**, *842*, 155813. [CrossRef]

32. Chen, T.; Guestrin, C. Xgboost: A scalable tree boosting system. In Proceedings of the 22nd ACM SIGKDD International Conference on Knowledge Discovery and Data Mining, Washington, DC, USA, 14 August 2022.

33. Husain, A.; Salem, A.; Jim, C.; Dimitoglou, G. Development of an Efficient Network Intrusion Detection Model Using Extreme Gradient Boosting (XGBoost) on the UNSW-NB15 Dataset. In Proceedings of the 2019 IEEE International Symposium on Signal Processing and Information Technology (ISSPIT), Ajman, United Arab Emirates, 1 December 2019.

34. Wan, Y.; Chen, F.; Fan, L.; Sun, D.; He, H.; Dai, Y.; Li, L.; Chen, Y. Conversion of surface CH4 concentrations from GOSAT satellite observations using XGBoost algorithm. *Atmos. Environ.* **2023**, *301*, 119694. [CrossRef]

35. Dong, J.; Zeng, W.; Wu, L.; Huang, J.; Gaiser, T.; Srivastava, A.K. Enhancing short-term forecasting of daily precipitation using numerical weather prediction bias correcting with XGBoost in different regions of China. *Eng. Appl. Artif. Intell.* **2023**, *117*, 105579. [CrossRef]

36. Liu, J.; Zhang, Q.; Xue, W.; Zhang, H.; Bai, Y.; Wu, L.; Zhai, Z.; Jin, G. Fluorescence Characteristics of Aqueous Synthesized Tin Oxide Quantum Dots for the Detection of Heavy Metal Ions in Contaminated Water. *Nanomaterials* **2019**, *9*, 1294. [CrossRef] [PubMed]

37. Liang, Y.; Wu, C.; Jiang, S.; Li, Y.J.; Wu, D.; Li, M.; Cheng, P.; Yang, W.; Cheng, C.; Li, L. Field comparison of electrochemical gas sensor data correction algorithms for ambient air measurements. *Sens. Actuators B Chem.* **2021**, *327*, 128897. [CrossRef]

38. Liu, J.; Lv, J.; Xiong, H.; Wang, Y.; Jin, G.; Zhai, Z.; Fu, C.; Zhang, Q. Size effect and comprehensive mathematical model for gas-sensing mechanism of SnO2 thin film gas sensors. *J. Alloys Compd.* **2022**, *898*, 162875. [CrossRef]

39. Liu, J.; Hu, J.; Liu, C.; Tan, Y.; Peng, X.; Zhang, Y. Mechanically exfoliated MoS2 nanosheets decorated with SnS2 nanoparticles for high-stability gas sensors at room temperature. *Rare Met.* **2021**, *40*, 1536–1544. [CrossRef]

40. Barreca, D.; Garon, S.; Tondello, E.; Zanella, P. SnO$_2$ Nanocrystalline Thin Films by XPS. *Surf. Sci. Spectra* **2000**, *7*, 81–85.

41. Cox, D.F.; Fryberger, T.B. Preferential isotopic labeling of lattice oxygen positions on the SnO2 (110) surface. *Surf. Sci.* **1990**, *227*, L105–L108. [CrossRef]

42. Matthews, H.; Kohnke, E. Effect of chemisorbed oxygen on the electrical conductivity of Zn-doped polycrystalline SnO2. *J. Phys. Chem. Solids* **1968**, *29*, 653–661. [CrossRef]

43. Xu, Y.; Zheng, L.; Yang, C.; Zheng, W.; Liu, X.; Zhang, J. Oxygen Vacancies Enabled Porous SnO2 Thin Films for Highly Sensitive Detection of Triethylamine at Room Temperature. *ACS Appl. Mater. Interfaces* **2020**, *12*, 20704–20713. [CrossRef] [PubMed]

44. Liu, J.; Liu, X.; Zhai, Z.; Jin, G.; Jiang, Q.; Zhao, Y.; Luo, C.; Quan, L. Evaluation of depletion layer width and gas-sensing properties of antimony-doped tin oxide thin film sensors. *Sens. Actuators B Chem.* **2015**, *220*, 1354–1360. [CrossRef]

45. Xu, C.; Tamaki, J.; Miura, N.; Yamazoe, N. Grain size effects on gas sensitivity of porous SnO2-based elements. *Sens. Actuators B Chem.* **1991**, *3*, 147–155. [CrossRef]

46. Yamazoe, N.; Shimanoe, K. New Perspectives of Gas Sensor Technology. *Sens. Actuators B Chem.* **2009**, *138*, 100–107. [CrossRef]

47. Yamazoe, N.; Shimanoe, K. Theory of power laws for semiconductor gas sensors. *Sens. Actuators B Chem.* **2008**, *128*, 566–573.

48. Inyawilert, K.; Punginsang, M.; Wisitsoraat, A.; Tuantranont, A.; Liewhiran, C. Graphene/Rh-doped SnO2 nanocomposites synthesized by electrochemical exfoliation and flame spray pyrolysis for H2S sensing. *J. Alloys Compd.* **2022**, *916*, 165431. [CrossRef]

49. Liu, Y.; Wang, X.; Zhao, Y.; Wu, Q.; Nie, H.; Si, H.; Huang, H.; Liu, Y.; Shao, M.; Kang, Z. Highly efficient metal-free catalyst from cellulose for hydrogen peroxide photoproduction instructed by machine learning and transient photovoltage technology. *Nano Res.* **2022**, *15*, 4000–4007. [CrossRef]